B. R. Baliga
Associate Professor.
Mem. ASME

R. R. Azrak
Former Graduate Student.

Department of Mechanical Engineering,
McGill University,
Montreal, Quebec H3A 2K6, Canada

Laminar Fully Developed Flow and Heat Transfer in Triangular Plate-Fin Ducts

This paper presents a numerical investigation of fully developed flow and heat transfer in triangular cross section plate-fin ducts encountered in compact heat exchangers. Heat conduction in the fin and convection in the fluid are analyzed simultaneously as a conjugate problem. Overall and local results are presented for representative values of the duct aspect ratio and a fin conductance parameter.

Introduction

Compact heat exchangers are characterized by a high ratio of heat transfer area to core volume, usually in excess of 700 m^2/m^3 [1]. Fins are commonly used between the plates in such heat exchangers to increase their compactness, and this practice often results in plate-fin flow passages of triangular cross section, as shown in Fig. 1. The heat transfer problem posed by such plate-fin ducts requires a simultaneous analysis of conduction in the fin and forced convection in the flow passage [2]. A numerical investigation of this conjugate problem is presented in this paper.

The plate-fin passages encountered in compact heat exchangers usually have small hydraulic diameters. This results in high area densities and high heat transfer coefficients, and the Reynolds number range for such passages, particularly for gases, usually falls well within the laminar flow regime [2]. Furthermore, with highly compact continuous plate-fin passages, such as those encountered in vehicular gas turbines, fully developed conditions can prevail over a substantial portion of the flow length [2]. In this paper, attention is limited to laminar fully developed flow and heat transfer in triangular plate-fin passages.

Laminar fully developed flow and heat transfer in ducts of triangular cross section have been analyzed by Kays [3], Schmidt and Newell [4], Nakamura et al. [5], Sparrow and Haji-Sheikh [6], Shah [7], Schneider and LeDain [8], and others. A comprehensive review of many of these investigations is available in a monograph by Shah and London [2]. The results of these investigations are useful in the design of plate-fin ducts, but they are strictly applicable only to fins of very high, or infinite, thermal conductance. In this investigation, fins of finite thermal conductance are considered. Thus the results presented in this paper complement and extend those in [2–8].

The importance of solving the conjugate problem in the analysis of heat transfer in finned ducts has been discussed by Shah and London [2], and demonstrated by Sparrow et al. [9] and Soliman et al. [10]. The mathematical model of the conjugate plate-fin duct problem presented in this paper is similar to that proposed in [9]. It is assumed in this model that longitudinal heat conduction (in the flow direction) is negligible in the plates, fins, and fluid. The influence of longitudinal conduction in a heat exchanger is to reduce its effectiveness for a given number of transfer units [1]. This reduction may be quite serious in heat exchangers with short flow lengths, but it is not expected to be serious in the fully developed flow regime analyzed in this paper. An analysis of this effect is available in [1].

Spatially averaged, or overall, and local results are presented in this paper. The overall results include friction factor–Reynolds number products and mean Nusselt numbers. The local results include velocity distribution in the fluid, and temperature and heat flux distributions along the plates and fins. The results depend on the duct aspect ratio and a fin conductance parameter. These parameters are assigned values that are representative of triangular plate-fin ducts commonly encountered in compact heat exchangers.

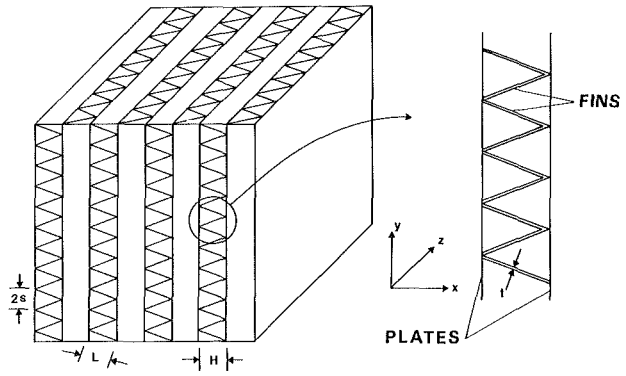

Fig. 1 Triangular plate-fin ducts encountered in compact heat exchangers

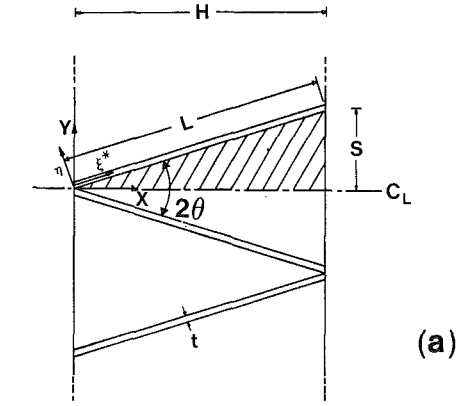

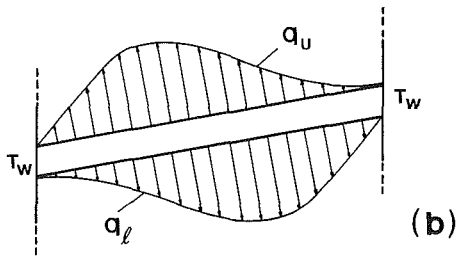

Fig. 2(a) Typical plate-fin duct cross section, showing the calculation domain and related nomenclature; (b) skew-symmetric heat flux distributions on the upper and lower fin-fluid interfaces

Contributed by the Heat Transfer Division for publication in the JOURNAL OF HEAT TRANSFER. Manuscript received by the Heat Transfer Division May 9, 1984. Paper No. 84-HT-55.

Problem Formulation

In a majority of compact heat exchangers, the plate-fin flow passages are very small compared to the overall core dimensions [1, 2]. In this analysis, therefore, it is assumed that the core is an infinite matrix of similar plate-fin passages, as shown in Fig. 1. Numerous symmetry surfaces exist in such a matrix. Furthermore, for any given fin in the central region of such a core, the fluid flow in the passages adjacent to its upper and lower surfaces is skew-symmetric; therefore, the heat flux distributions on its two surfaces are skew-symmetric, as is qualitatively illustrated in Fig. 2(*b*). Advantage is taken of these features to limit the calculation domain to only 1/4 of the total cross-sectional area between two similar fins, as shown by the shaded region in Fig. 2(*a*).

Two types of thermal boundary conditions are considered in this analysis. In one, the temperature of the plates T_w is assumed to be constant, both in the streamwise direction and in any cross section: The symbol (T) will be used to denote this boundary condition. In the other, a uniform rate of heat input per unit length Q' is prescribed, and the plates are regarded as being highly conductive, or sufficiently thick, so that their temperature T_w is uniform in any cross section but varies axially: This boundary condition will be denoted by the symbol (HI). In both these categories of the problem of interest, the fin temperature distribution T_f is determined by conduction within the fin and convection in the fluid. At the fin-plate interface, it is assumed that $T_f = T_w$. In practice, however, because the rate of heat transfer at the plate-fin interface is usually much greater than that passing through a comparable area on the unfinned portion of the plate, the temperature at the plate-fin interface may be depressed relative to that of the surrounding plate material. Sparrow and Lee [11] have shown that this base temperature depression could result in a significant decrease in the fin heat transfer relative to that predicted by a model which neglects this base temperature depression, but its influence on the total (fin + plate) rate of heat transfer is not as serious. Furthermore, for a fixed plate area, as the number of fins increases, the effect of the base temperature depression becomes progressively less important [11]. Heggs and Stones [12] have also investigated this problem, using a two-dimensional model of heat conduction in the fin. It should also be noted that the (T) and (HI) boundary conditions imposed on the plates may not correspond to those encountered in practice, but they represent extreme or bounding cases of the actual conditions in compact heat exchangers [1, 2, 13].

As shown in Fig. 2(*a*), the spacing between the plates is denoted by H, s is half the distance between adjacent fin attachment points on any given plate, L is the length of the fin, and the fin thickness is denoted by t. Two Cartesian coordinate systems, (x, y) and (ξ^*, η^*), are used in the analysis: The x axis is aligned along the centerline between two adjacent fins, and the ξ^* axis is oriented along the fin. Mathematical descriptions of the fluid flow and heat transfer problems of interest are presented in the remainder of this section in terms of the following dimensionless coordinates and geometrical parameters

$$X=x/H;\ Y=y/H;\ \xi=\xi^*/H;\ \eta=\eta^*/H$$
$$Z=(z/H)/(\bar{w}H/\alpha);\ \zeta=H/s \tag{1}$$

where α is the thermal diffusivity of the fluid ($\alpha=k/\rho c_p$), and ζ is the aspect ratio of the plate-fin duct.

Fluid Flow. In the fully developed region, $u=v=0$, $w=w(x, y)$, p is uniform in any given cross section, dp/dz is constant, and for a constant-property Newtonian fluid flow, the z-momentum equation reduces to

$$\partial^2 W/\partial X^2+\partial^2 W/\partial Y^2+1=0 \tag{2}$$

where W is a nondimensional axial velocity

$$W=\frac{w}{(H^2/\mu)(-dp/dz)} \tag{3}$$

The boundary conditions on W are the following: At $X=1$, or along the plate, $W=0$; along the centerline, or $Y=0$, $\partial W/\partial Y=0$; and along the fin, or $X=\zeta Y$, $W=0$.

Heat Transfer: (T) Boundary Condition. In this category of problems, the thermally fully developed region is characterized by a dimensionless temperature distribution that remains invariant with the streamwise coordinate [2, 3]

$$(T_W-T)/(T_W-T_b)=\theta(X, Y) \tag{4a}$$

where T_b is the fluid bulk temperature. In the thermally fully developed region, the difference between T_b and T_w decays exponentially with z, so that

$$\{d(T_w-T_b)/dZ\}/(T_w-T_b)=\text{const}=-\lambda \tag{4b}$$

Nomenclature

a, b = constants in interpolation function for ϕ_f, equation (23)
A, B, C = constants in interpolation function for ϕ, equation (22)
a_i, a_n, b_i = constants in discretization equation, equation (24)
c_i, d_i, e_i, f_i = constants in discretization equation, equation (25)
c_p = specific heat at constant pressure, J/kg•K
D_H = hydraulic diameter, equation (27), m
f = Darcy friction factor, equation (26)
h = heat transfer coefficient, equation (28), W/m²•K
H = spacing between plates, Fig. 2(*a*), m
i = index in fin node numbering scheme, Fig. 4(*b*)
I, J = indices in node numbering scheme, Fig. 3
k = thermal conductivity, for fluid if no subscript, W/m•K
L = length of the fin, Fig. 2(*a*), m
£ = nondimensional fin length $=L/H$
M = total number of nodes along the centerline, $Y=0$
N = total number of nodes along the plate, $X=1$
Nu = Nusselt number, equation (28)
p = pressure, N/m²
q = heat flux, W/m²
q_u = heat flux on the upper fin-fluid interface, Fig. 2(*b*), W/m²
q_l = heat flux on the lower fin-fluid interface, Fig. 2(*b*), W/m²
q_p = heat flux to the fluid at the plate–fluid interface, W/m²
$\bar{q}_l, \bar{q}_p$ = mean values of q_l and q_p, respectively, W/m²
Q = total surface-integrated heat loss over the fin and the plate, W/m
Q_f = surface-integrated heat loss over the fin, W/m
Q' = constant rate of heat transfer to the fluid per unit axial length, equation (15), W/m
Re = Reynolds number, equation (26)
s = half-distance along the plate between successive plate-fin junctions, Fig. 2(*a*), m

Noting that $u=v=0$, and neglecting longitudinal heat conduction and viscous dissipation, the energy equation in the fluid reduces to the following

$$\rho w c_p \frac{\partial T}{\partial z} = k\left(\frac{\partial^2 T}{\partial x^2} + \frac{\partial^2 T}{\partial y}\right) \tag{5a}$$

In terms of θ, λ, and the dimensionless variables defined in equation (1), it can be shown that

$$\rho w c_p (\partial T/\partial z) = k(T_w - T_b)(W/\bar{W})\lambda\theta/H^2$$

$$(\partial^2 T/\partial x^2) = -(T_w - T_b)(\partial^2\theta/\partial X^2)/H^2;$$

$$(\partial^2 T/y^2) = -(T_w - T_b)(\partial^2\theta/\partial Y^2)/H^2 \tag{5b}$$

and equation (5*a*) can be rewritten as follows

$$\partial^2\theta/\partial X^2 + \partial^2\theta/\partial Y^2 + \lambda(W/\bar{W})\theta = 0 \tag{6}$$

At $X=1$, or along the plate, $\theta=0$; and along the centerline, or $Y=0$, $(\partial\theta/\partial Y)=0$. The normalized velocity distribution $(W/\bar{W})$ in equation (6) is obtained from the fluid flow analysis.

At any location ξ^* along the fin, there is a balance between the net conduction along the fin and the heat transfer from the surface of the fin to the fluid. In the context of a one-dimensional model of the fin, this energy balance can be expressed as

$$k_f t(d^2 T_f/d\xi^{*2}) = q_u + q_l \tag{7}$$

where the subscript f refers to the fin, and q_u and q_l are the heat fluxes on the upper and lower surfaces of the fin, respectively

$$q_u = -k(\partial T/\partial\eta^*)_u;\ q_l = k(\partial T/\partial\eta^*)_l \tag{8}$$

In this equation, the temperature gradients correspond to those on the fluid side of the fin-fluid interfaces, and k is the thermal conductivity of the fluid. With reference to the skew-symmetric heat flux distributions shown in Fig. 2(*b*), it can be established that q_u and q_l are related by the following equation

$$q_u\Big|_{\xi^*} = q_l\Big|_{L-\xi^*} \tag{9}$$

Advantage is taken of this relationship between q_u and q_l to limit the calculation domain to the shaded region shown in Fig. 2(*a*). In dimensionless terms, equations (7–9) can be combined and expressed as follows

$$\Omega(d^2\theta_f/d\xi^2) = [(\partial\theta/\partial\eta)_\xi + (\partial\theta/\partial\eta)_{\pounds-\xi}] \tag{10}$$

where $(\partial\theta/\partial\eta)$ is the normal gradient of θ in the fluid on the lower surface of the fin, the subscript l has been dropped for compactness in the presentation; $\pounds = (L/H) = [1+(1/\zeta)^2]^{1/2}$; and Ω is the fin conductance parameter, given by

$$\Omega = (k_f t)/(kH) \tag{11}$$

At $\xi=0$ and at $\xi=\pounds$, $\theta_f=0$.

For any given set of ζ and Ω, equations (6) and (10), along with the aforementioned boundary conditions, pose an eigenvalue problem. The eigenvalue λ has to be found so that the solution satisfies the following requirement, which follows from the definition of the bulk temperature

$$2\zeta\iint(W/\bar{W})\theta dX dY = 1 \tag{12}$$

where the integration is carried out over the shaded region in Fig. 2(*a*).

In the solution of this eigenvalue problem, it is convenient to define a variable ψ as follows

$$\psi = \theta/\lambda;\ \phi_f = \psi_f/\lambda \tag{13}$$

In terms of ϕ, equations (6) and (10), and the associated boundary conditions, remain unchanged, and equation (12) yields

$$\lambda = 1/\{2\zeta\iint(W/\bar{W})\psi dX dY\} \tag{14}$$

An iterative numerical method is used to solve this conjugate heat transfer problem. Details of this method are presented later in this paper.

Heat Transfer: (H1) Boundary Condition. In this problem, a uniform rate of heat input per unit axial length Q' is prescribed, and the plate temperature T_w is assumed to be uniform in each cross section but varies axially. With this boundary condition, and assuming that viscous dissipation is negligible, all temperatures vary linearly with axial distance in the thermally developed region, and an overall energy balance yields the following

$$\partial T/\partial z = dT_b/dz = dT_w/dz = 2Q'/(\rho\bar{w}Hsc_p) \tag{15}$$

Furthermore, in the thermally developed regime, the following dimensionless temperature remains invariant with the streamwise coordinate [2, 3]

$$(T_w - T)/(Q'/k) = \tau(X, Y) \tag{16}$$

Nomenclature (cont.)

S = volumetric source term, equation (19)
t = fin thickness, Fig. 2(*a*), m
T = temperature, K
T_b = fluid bulk temperature, K
T_f = temperature inside the fin, K
T_w = plate temperature, K
u, v, w = fluid velocity components in the x, y, and z directions, respectively, m/s
W = dimensionless axial velocity of the fluid, equation (3)
$\bar{w}, \bar{W}$ = mean values of w and W, respectively
x, y, z = Cartesian coordinates, Figs. 1 and 2(*a*), m
X, Y, Z = nondimensional coordinates, equation (1)
α = thermal diffusivity = $k/\rho c_p$, m^2/s
ζ = aspect ratio = H/s
$\eta_{0,\text{prop}}$ = total (fin + plate) surface efficiency obtained using the proposed conjugate analysis, equation (33)
$\eta_{0,\text{conv}}$ = total (fin + plate) surface efficiency obtained using conventional analysis, equation (31)
θ = nondimensional temperature, equation (4)
Θ = half-angle between adjacent fins, Fig. 2(*a*), deg
λ = eigenvalue, equations (4*a*) and (14)
μ = dynamic viscosity of the fluid, kg/m•s
ξ^*, η^* = Cartesian coordinates, Fig. 2(*a*), m
ξ, η = nondimensional coordinates, equation (1)
ρ = mass density of the fluid, kg/m^3
τ = dimensionless temperature, equation (16)
ψ = dimensionless temperature = θ/λ
ϕ = general scalar dependent variable, equation (19)
Ω = fin conductance parameter, equation (11)

Subscripts

$a, b, c, 0$ = values pertaining to specific locations in the domain discretization, Fig. 4(*a*)
e, w = control volume face locations in the fin discretization, Fig. 4(*b*)
f = values or variables pertaining to the fin
H1 = pertaining to the thermal boundary condition of prescribed Q'
T = pertaining to the thermal boundary condition of prescribed T_w

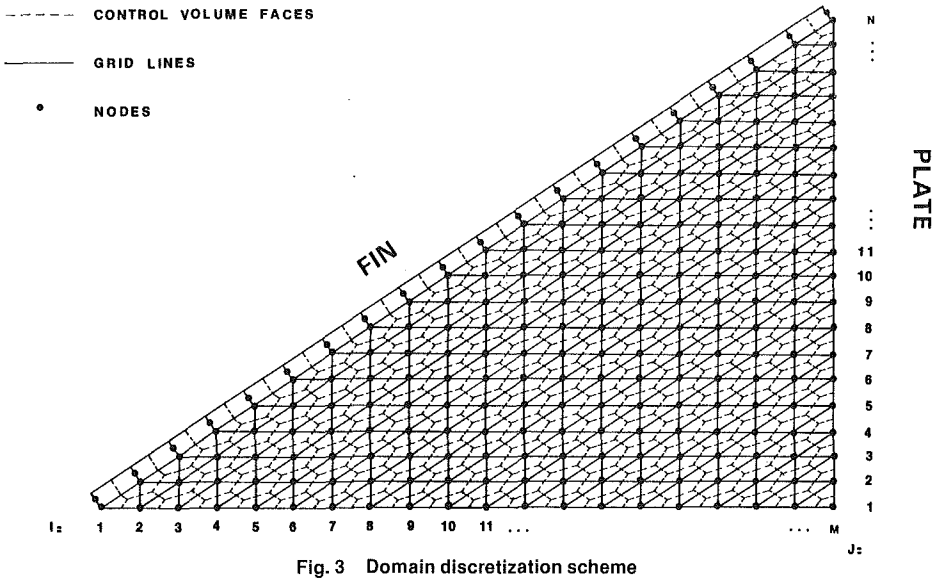

Fig. 3 Domain discretization scheme

Using equations (15) and (16), the energy equation (5*a*) in the fluid can be written in the following dimensionless form

$$\partial^2\tau/\partial X^2 + \partial^2\tau/dY^2 + 2\zeta(W/\bar{W}) = 0 \tag{17}$$

At $X=1$, or along the plate, $\tau=0$; and along the centerline, or $Y=0$, $\partial\tau/\partial Y=0$. The normalized velocity distribution $(W/\bar{W})$ in equation (17) is obtained from the fluid flow analysis.

The thermal analysis of the fin is similar to that presented in the previous section, and the governing equation for τ_f is the following

$$\Omega(d^2\tau_f/d\xi^2) = [(\partial\tau/\partial\eta)_{\xi} + (\partial\tau/\partial\eta)_{\pounds-\xi}] \tag{18}$$

where Ω is the fin conductance parameter given by equation (11), and $(\partial\tau/\partial\eta)$ is the normal gradient of τ in the fluid on the lower surface of the fin; the right side of equation (18) reflects the skew-symmetric distributions of the heat flux at the upper and lower fin-fluid interfaces, as shown in Fig. 2(*b*). At $\xi=0$ and at $\xi=\pounds$, $\tau_f=0$.

Equations (17) and (18), subject to the aforementioned boundary conditions, were solved by an iterative numerical method described in the next section.

Numerical Method

A control volume finite element method was used to solve the mathematical models described in the previous section. This method is briefly described in this section; a detailed description of the method is available in [14].

Domain Discretization. The shaded region in Fig. 2(*a*) is first discretized into three-node triangular elements. Then the centroids of the elements are joined to the midpoints of the corresponding sides to create polygonal control volumes surrounding each node in the calculation domain. A sample domain discretization is shown in Fig. 3; the solid lines denote the domain and element boundaries, and the dashed lines represent the control volume faces. The nodes along the centerline, $Y=0$, are numbered $I=1, 2, 3, \ldots, M$; and along the plate, $X=1$, the nodes are numbered $J=1, 2, 3, \ldots, N$. In all discretizations used in this investigation, the same number of nodes was used along the centerline, the plate and the fin boundary: $M=N$ in all cases. Thus the nodes in the proposed discretization scheme are arranged in a line-by-line pattern, with the lines parallel to the sides of the triangular calculation domain. This arrangement of nodes facilitates the storage, assembly, and solution of the discretization equations.

The fin is discretized into control volumes and nodes which are compatible with the discretization of the flow passage, as illustrated in Fig. 3.

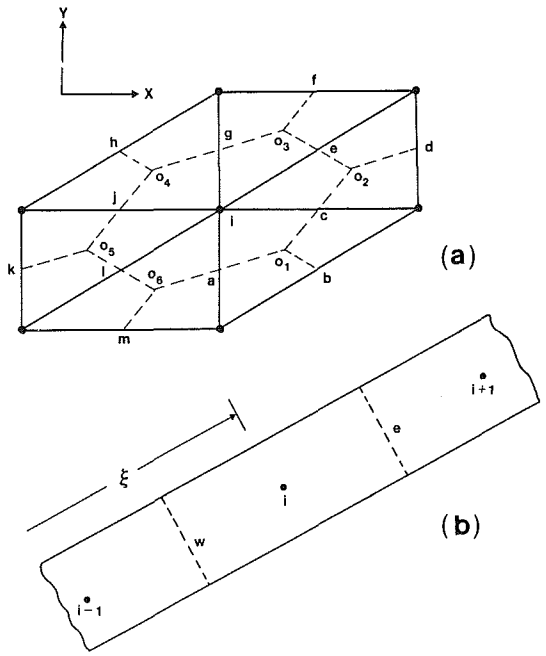

Fig. 4 Details of the discretization of (*a*) the flow passage, and (*b*) the fin

Conservation Equation for a Control Volume. Equations (2), (6), and (17) can be integrated over a control volume V and cast in the following general form

$$\int_{\partial V} \nabla\phi \cdot \mathbf{n}\, ds + \int_V S\, dV = 0 \tag{19}$$

where ϕ is a general scalar dependent variable, S is interpreted as a volumetric source term, ∂V is the surface of the control volume, and $\mathbf{n}$ is a unit outward normal to the differential area element ds. The fluid flow problem can be modeled by setting $\phi=W$ and $S=1$; the (T) heat transfer problem can be simulated by setting $\phi=\psi$ and $S=\lambda(W/\bar{W})\psi$; and by setting $\phi=\tau$ and $S=2\zeta(W/\bar{W})$, the (H1) heat transfer problem can be modeled.

When applied to the polygonal control volume associated with a typical node i, such as the one shown in Fig. 4(*a*), equation (19) can be written as follows

Table 1 Overall fluid flow results

ζ	Angle $\gtrless 2\theta$	f.Re [Present]	f.Re [2]	f.Re [8]
11.430	10°	50.188	49.90	50.044
3.732	30°	52.520	52.26	52.346
1.732	60°	53.744	53.33	53.360
1.000	90°	52.936	52.61	52.645
0.577	120°	51.224	50.98	50.970

Table 2 Comparison of average Nusselt numbers for $\Omega = \infty$

ζ	Nu_T [Present]	Nu_T [8]	Nu_{H1} [Present]	Nu_{H1} [8]
11.430	1.726	1.700	2.467	2.437
3.732	2.284	2.274	2.921	2.910
1.732	2.500	2.497	3.110	3.111
1.000	2.359	2.358	2.979	2.983
0.577	2.031	2.029	2.681	2.684

$$\left[\int_a^{0_1} \nabla\phi\cdot\mathbf{n}ds + \int_{0_1}^{c} \nabla\phi\cdot\mathbf{n}ds - \int_{ia0_1c} SdV\right] \tag{20}$$

+ [Similar contributions from other elements associated with node i]
+ [Boundary contributions, if applicable] = 0

This form of the conservation equation emphasizes that it can be assembled using an element-by-element procedure.

Similarly, the fin equations (10) and (18) can be integrated over the control volume associated with a typical fin node i, such as the one shown in Fig. 4(*b*), and cast in the following general form

$$\Omega[(d\phi_f/d\xi)_e - (d\phi_f/d\xi)_w] = \left[\int_w^e (\partial\phi/\partial\eta)_\xi d\xi + \int_w^e (\partial\phi/d\eta)_{\xi-\xi} d\xi\right] \tag{21}$$

Interpolation Functions. In the flow passage, all dependent variables are interpolated linearly in each three-node triangular element

$$\phi = AX + BY + C \tag{22}$$

the constants A, B, and C in this interpolation function can be uniquely determined in terms of the nodal coordinates and the corresponding values of ϕ.

In the fin, the dependent variables are interpolated by piecewise linear functions in ξ. Thus between any two adjacent nodes

$$\phi_f = a\xi + b \tag{23}$$

where a and b are unique functions of the nodal values of ξ and ϕ_f.

Discretization Equations. The interpolation functions given by equations (22) and (23) are used to obtain algebraic approximations to the integrals and derivatives in equations (20) and (21). The area and line integrals involved in this derivation are quite straightforward [14, 15], so the details will not be presented here.

In a general form, the discretization equation for a node i in the flow passage can be expressed as follows

$$a_i\phi_i = \sum_n a_n\phi_n + b_i \tag{24}$$

where the summation is taken over all neighbors of node i. Similarly, a general representation of the discretization equation for a node i in the fin is

$$c_i(\phi_f)_i = d_i(\phi_f)_{i+1} + e_i(\phi_f)_{i-1} + f_i \tag{25}$$

Solution of the Discretization Equations

Fluid Flow. In the fluid flow problem, $\phi = W$ and $S = 1$, and equation (24) represents a set of simultaneous, linear algebraic equations. In this investigation, these equations were solved by a line-by-line iterative method based on the *Tri-Diagonal-Matrix-Algorithm* (TDMA). Details of this method are available in [16]. It should be noted here that this scheme can be used because the proposed domain discretization scheme provides a line-by-line arrangement of the nodes. In all cases considered in this analysis, the iterations were terminated when all values of W had converged to at least five significant figures.

Heat Transfer: (T) *Problem.* In this case, $\phi = \psi$, $S = \lambda(W/\bar{W})\psi$, and $\phi_f = \psi_f$. The normalized velocity distribution $(W/\bar{W})$ in this problem is obtained by solving the aforementioned fluid flow problem first. Equations (24) and (25) represent a coupled set of simultaneous linear algebraic equations which, together with equation (14), pose an eigenvalue problem. The following iterative procedure was used to solve this problem: (1) guess all unknown nodal values of ϕ; (2) using this ϕ distribution, calculate the coefficients in equation (25), and solve this set of equations, using TDMA, to obtain the fin temperature distribution ϕ_f; (3) with the available ϕ distribution, calculate λ using equation (14); (4) with this value of λ, and using the available ϕ_f values as boundary conditions at the fluid-fin interface, solve equation (24), using a line-by-line iterative method, to obtain a new ϕ distribution; (5) return to step 2, and repeat until all ϕ values and the value of λ have converged to at least five significant figures; and (6) calculate the θ distribution, using $\theta = \lambda\phi$.

Heat Transfer: (H1) *Problem.* In this problem, $\phi = \tau$, $S = 2\zeta(W/\bar{W})$, and $\phi_f = \tau_f$. Again $(W/\bar{W})$ is obtained from the fluid flow analysis, and equations (24) and (25) represent a coupled set of simultaneous linear algebraic equations. The following iterative procedure was used to solve this set of equations: (1) Guess all unknown nodal values of ϕ; (2) using this ϕ distribution, calculate the coefficients in equation (25) and solve this set of equations, using TDMA, to obtain the fin temperature distribution ϕ_f; (3) using the available ϕ_f values as boundary conditions at the fluid-fin interface, solve equation (24), using a line-by-line iterative method, to obtain

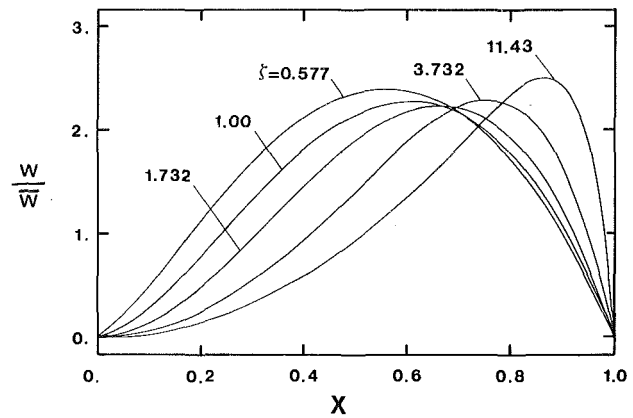

Fig. 5 Normalized velocity distributions along the symmetry boundary ($Y=0$) for different aspect ratios

a new ϕ distribution; (4) return to step 2 and repeat until all ϕ values have converged to at least five significant figures.

Results

The numerical method described in the previous section was used to study fully developed flow and heat transfer in a total of thirty different triangular plate-fin ducts; five values of the aspect ratio were considered, $\zeta = 11.43$, 3.732, 1.732, 1.0, and 0.577; for each of these aspect ratios, six values of the fin conductance parameter were investigated, $\Omega = \infty$, 25, 10, 5, 2, and 1. These values of ζ and Ω are characteristic of air flows in commonly encountered triangular plate-fin passages.

Numerous preliminary runs were undertaken to (1) establish the validity of the computer implementation of the proposed numerical method, and (2) obtain grid configurations that provide a satisfactory balance between the accuracy and the computational cost of the results. The final choice for $\zeta > 1.732$ was a 325-node (625-element) grid with a moderate stacking of nodes adjacent to the solid boundaries: the spacing of successive grid points along $Y=0$, moving away from the point $X=0$ toward the centroid of the triangular flow passage, was given by $(X_{i+1}/X_i) = \{(i+1)/i\}^{1.2}$, and similar grid spacing was used in the vicinity of other solid boundaries. For $\zeta \leqq 1.732$ a 190-node (361-element) uniform grid was used.

The results of this study can be grouped into two main categories: overall results and local results. These two categories of results are presented and discussed next in this section. Following that, the results of this study are used to evaluate the validity of the conventional approach to the design of plate-fin ducts.

Overall Results

Fluid Flow: Overall fluid flow results will be presented in terms of the product of the Darcy friction factor and the Reynolds number

$$f \cdot \mathrm{Re} = \left\{ \frac{(-dp/dz) D_h}{\rho \bar{w}^2/2} \right\} \left(\frac{\rho \bar{w} D_h}{\mu} \right) = \frac{8}{[(\zeta^2+1)^{1/2}+1]^2 \bar{W}} \quad (26)$$

where D_h is the hydraulic diameter

$$D_h = (2Hs)/[(H^2+s^2)^{1/2}+s] \quad (27)$$

The values of $f \cdot \mathrm{Re}$ obtained in this study and those reported in [2, 8] are presented in Table 1. Good agreement between the results is evident in all cases.

Heat Transfer Results: The overall heat transfer characteristics of the triangular plate-fin ducts will be presented in terms of the average Nusselt number Nu and the ratio Q_f/Q; with reference to Fig. 2, Q_f is the surface-integrated heat loss from the lower surface of the fin to the fluid, and Q is the sum of Q_f and the heat loss from the plate to the fluid over the range $0 \leqq y \leqq s$. The average Nusselt number was evaluated as follows

$$h = \frac{Q/(T_w - T_b)}{(H^2+s^2)^{1/2}+s}; \quad \mathrm{Nu} = \frac{hD_h}{k} \quad (28)$$

In Table 2, the values of Nu_T and Nu_{HI} for $\Omega = \infty$ are compared with those reported in [8]. In all cases, the agreement between the results is good.

All overall heat transfer results are presented in Table 3. For all aspect ratios, Nu_T and Nu_{HI} decrease monotonically as the fin conductance parameter Ω decreases. This indicates that for a fixed plate-fin geometry, a decrease in fin thermal conductivity lowers the average heat transfer coefficient h defined in equation (28). The ratio Q_f/Q decreases as Ω decreases for a fixed aspect ratio. This is because low fin thermal conductivities lead to low values of Q_f. For a fixed value of Ω, Q_f/Q increases with aspect ratio. The reason for this is that for high aspect ratios, the fin surface area constitutes the major part of the overall heat transfer area. It is to be noted that the Nu values for the (T) problem are consistently lower than the corresponding values for the (HI) problem; this is consistent with the results for $\Omega = \infty$ reported in [2, 8].

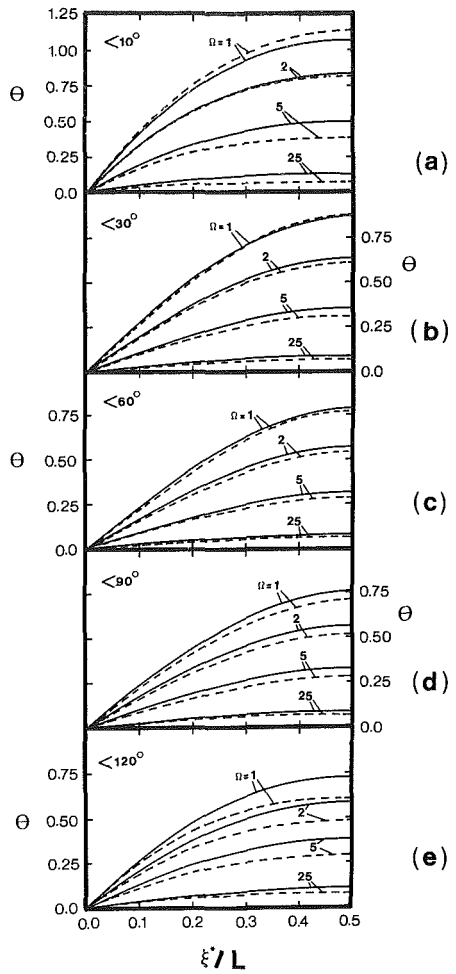

Fig. 6 Nondimensional fin temperature distribution (——— (HI); ..... (T)): (a) $\zeta = 11.43$; (b) $\zeta = 3.732$; (c) $\zeta = 1.732$; (d) $\zeta = 1.00$; (e) $\zeta = 0.577$

Local Results

Nondimensional Velocity Distribution: Dimensionless velocity distributions ($W/\bar{W}$) along the symmetry boundary ($Y=0$) between two adjacent fins are presented in Fig. 5. These distributions are strongly influenced by the aspect ratio

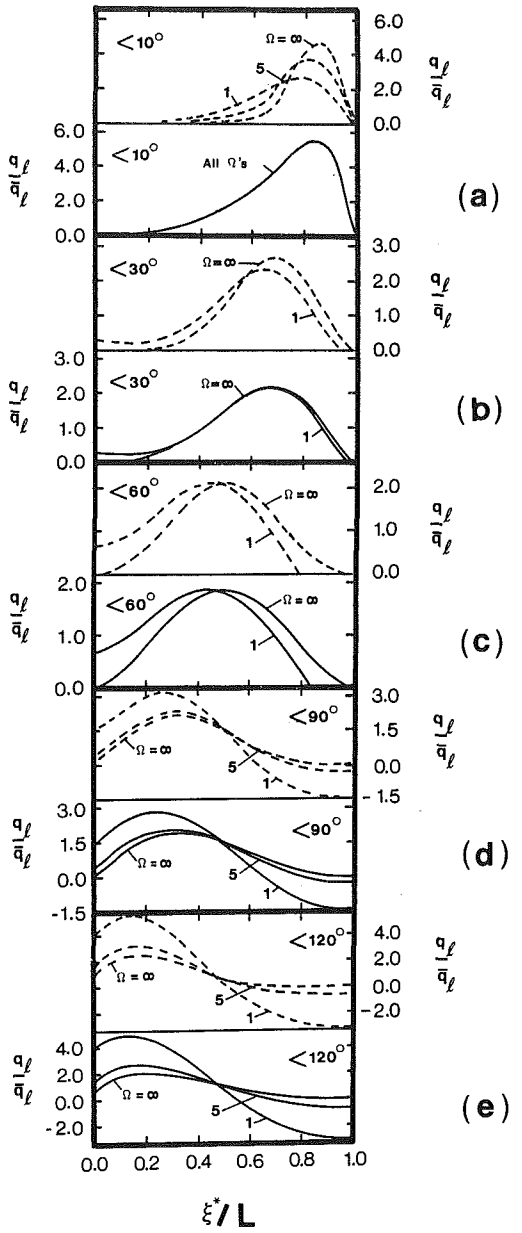

Fig. 7 Nondimensional heat flux distribution on the lower fin-fluid interface (——— (HI) ; ····· (T)): (a) $\zeta = 11.43$; (b) $\zeta = 3.732$; (c) $\zeta = 1.732$; (d) $\zeta = 1.00$; (e) $\zeta = 0.577$

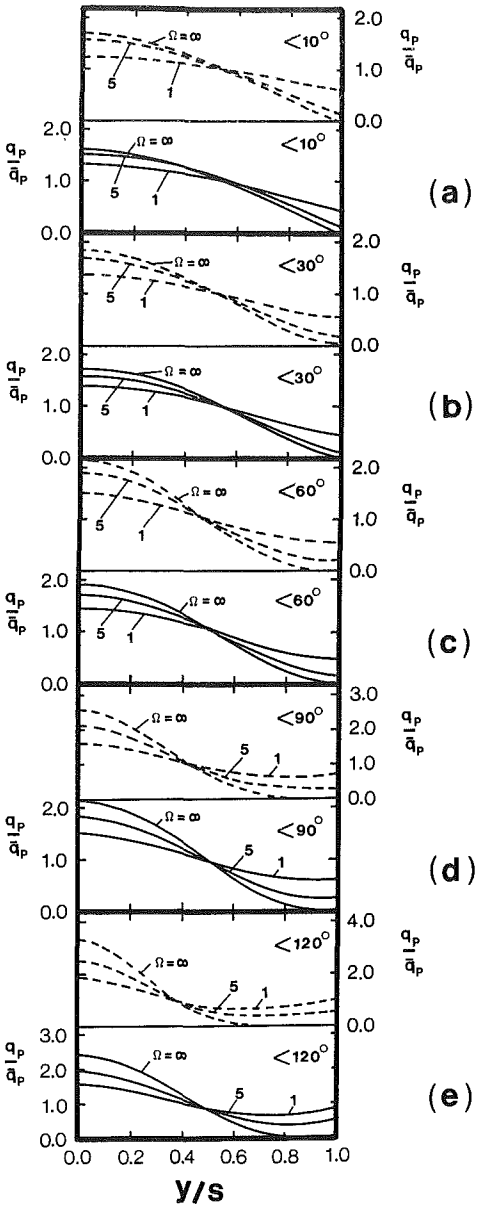

Fig. 8 Dimensionless heat flux distribution on the plate-fluid interface (——— (HI) ; ····· (T)): (a) $\zeta = 11.43$; (b) $\zeta = 3.732$; (c) $\zeta = 1.732$; (d) $\zeta = 1.00$; (e) $\zeta = 0.577$

ζ. Furthermore, the maxima do not occur at the centroids of the triangular plate-fin passages, except when the passage is equilateral ($\zeta = 1.732$). The location of the maximum velocity point shifts toward the plate ($X = 1$) as the aspect ratio is increased. This is because the fluid flow seeks the path of least resistance; it is to be noted that the location of the maxima in Fig. 5 agree well with the corresponding results in [2]. Another interesting feature of the plots in Fig. 5 is that the maximum value of $(W/\bar{W})$ for the equilateral passage ($\zeta = 1.732$) is lower than that of other ducts. This indicates that for $\zeta = 1.732$, the W distribution over the cross section of the duct is not as nonuniform as that for other values of ζ.

Nondimensional Fin Temperature: Distributions of $(T_w - T_f)/(T_w - T_b)$ are presented in Figs. 6(*a–e*). Results for both the (T) and (HI) thermal boundary conditions are plotted on the same graphs, the former being shown by dashed lines and the latter by solid lines. Each graph corresponds to a particular value of ζ and is parametrized by values of Ω. It is to be noted that for all cases, the two end temperatures of the fin are T_w, and the heat flux distributions on the upper and lower fin-fluid interfaces are skew-symmetric. Therefore, the total surface heat flux $(q_u + q_l)$ and the fin temperature distribution are symmetric about the center point of the fin; thus the range of the abscissa in Fig. 6 is $0 \leqq \xi^*/L \leqq 0.5$.

The curves corresponding to $\Omega = \infty$ coincide with the abscissa in all graphs. For a finite Ω, T_f drops from T_w at the ends of the fin to its lowest value at the midpoint. This causes $(T_w - T_f)/(T_w - T_b)$ to increase from zero at $(\xi^*/L) = 0$ to its maximum value at $(\xi^*/L) = 0.5$. For a given aspect ratio, this increase in $(T_w - T_f)/(T_w - T_b)$ gets more pronounced as Ω is decreased; this implies that for a fixed T_w, or a given axial location along the duct, as Ω decreases, the drop in T_f exceeds that in T_b. Another feature of the plots in Fig. 6 is that the temperature drop along the fin increases, consistently, with an increase in the aspect ratio. This may be explained by noting that an increase in aspect ratio ζ can be viewed as an increase in the fin length L for a fixed value of s; hence a larger temperature drop at its center, which is now farther from the plates, is to be expected.

For $\zeta = 11.43$ and $\Omega = 1$, it is seen that $\{(T_w - T_f)/(T_w -$

Table 3 Overall heat transfer results

ζ	Ω	Nu_T	Nu_{H1}	$(Q_f/Q)_T$	$(Q_f/Q)_{H1}$
11.430	∞	1.726	2.467	0.88	0.905
	25	1.676	2.254	0.88	0.902
	10	1.594	1.997	0.88	0.898
	5	1.450	1.682	0.88	0.890
	2	1.065	1.154	0.88	0.869
	1	0.710	0.774	0.87	0.836
3.732	∞	2.284	2.921	0.770	0.781
	25	2.210	2.761	0.768	0.773
	10	2.105	2.555	0.765	0.762
	5	1.944	2.283	0.758	0.744
	2	1.575	1.770	0.726	0.695
	1	1.218	1.348	0.666	0.627
1.732	∞	2.500	3.110	0.668	0.668
	25	2.424	2.972	0.658	0.654
	10	2.322	2.797	0.643	0.634
	5	2.174	2.564	0.619	0.605
	2	1.862	2.124	0.552	0.530
	1	1.574	1.762	0.464	0.441
1.000	∞	2.359	2.979	0.600	0.595
	25	2.299	2.859	0.581	0.573
	10	2.220	2.711	0.555	0.544
	5	2.110	2.521	0.515	0.501
	2	1.890	2.184	0.424	0.407
	1	1.701	1.924	0.328	0.312
0.577	∞	2.301	2.681	0.553	0.545
	25	1.987	2.563	0.519	0.507
	10	1.931	2.431	0.475	0.459
	5	1.861	2.280	0.417	0.398
	2	1.738	2.053	0.309	0.289
	1	1.647	1.907	0.221	0.204

$T_b)\}>1$ in the vicinity of the midpoint of the fin; this indicates that in the central region of the fin, its temperature falls below the fluid bulk temperature. The plots in Fig. 6 also indicate that the dimensionless fin temperatures for the (T) and (H1) boundary conditions differ only slightly.

Dimensionless Fin Heat Flux: Distributions of $q_l/\bar{q}_l$ are presented in Figs. 7($a-e$), for both the (T) (dashed lines) and the (H1) (solid lines) boundary conditions. For each of the aspect ratios considered, the plots in Fig. 7 are parametrized by the fin conductance parameter Ω; to avoid excessive crowding, however, the results for certain values of Ω have been omitted.

In all cases, the $q_l/\bar{q}_l$ distribution varies markedly along the fin. All $q_l/\bar{q}_l$ plots are significantly affected by the values of ζ and Ω. For fixed values of Ω, as ζ decreases, the location of the maxima of $q_l/\bar{q}_l$ shifts away from the vicinity of the plate at $X=1$, and moves toward the end at $X=0$. This is in response to similar changes in the location of the maxima of the fluid velocity distribution. For a fixed aspect ratio, it is expected that as Ω decreases, q_l decreases. In Fig. 7, however, it is seen that for $\zeta<1.732$, the maxima in $q_l/\bar{q}_l$ increase as Ω decreases; this indicates that the decrease in $\bar{q}_l$ is faster than that in the maximum value of q_l.

In Fig. 2(b), the heat flux distributions on the lower and upper surfaces of the fin are shown to be skew-symmetric and positive. From the plots in Fig. 7, however, it is seen that $q_l/\bar{q}_l$ takes on negative values in the region adjacent to the plate at $(\xi^*/L)=1$, for $\zeta<11.43$ and small values of Ω. This phenomenon, which may appear surprising at first, is physically meaningful. Using the information in Fig. 7 and noting that q_u and q_l are skew-symmetric, it can be deduced that the algebraic sum (q_u+q_l) is always positive. Thus the net heat transfer is always from the fin to the fluid. The negative part of the heat flux distribution on the individual fin surfaces implies, therefore, that the hot fluid in the corners formed by the fins and the plates transfers energy, *via the fin*, to the relatively less hot fluid in the corners formed by adjacent fins. In the context of compact heat exchanger design, therefore, it may be concluded that combinations of ζ and Ω, which give rise to negative values of $q_l/\bar{q}_l$, are not thermally efficient.

Table 4 Total surface efficiencies obtained with the conventional and the proposed analyses

		(T)			(H1)		
ζ	Ω	$\eta_{o,conv}$	$\eta_{o,prop}$	% Error	$\eta_{o,conv}$	$\eta_{o,prop}$	% Error
11.430	∞	1.000	1.000	0.00	1.000	1.000	0.00
	25	0.939	0.971	- 3.30	0.915	0.914	0.11
	10	0.863	0.924	- 6.60	0.818	0.809	1.11
	5	0.768	0.840	- 8.57	0.706	0.682	3.52
	2	0.599	0.617	- 2.92	0.530	0.468	13.25
	1	0.468	0.411	13.87	0.408	0.314	29.94
3.732	∞	1.000	1.000	0.00	1.000	1.000	0.00
	25	0.970	0.968	0.21	0.962	0.945	1.80
	10	0.930	0.922	0.87	0.912	0.875	4.23
	5	0.873	0.851	2.59	0.845	0.782	8.06
	2	0.752	0.690	8.99	0.713	0.606	17.66
	1	0.638	0.533	19.70	0.597	0.461	29.50
1.732	∞	1.000	1.000	0.00	1.000	1.000	0.00
	25	0.979	0.970	0.93	0.974	0.956	1.88
	10	0.949	0.929	2.15	0.939	0.899	4.45
	5	0.907	0.870	4.25	0.889	0.824	7.89
	2	0.814	0.745	9.26	0.786	0.683	15.08
	1	0.721	0.630	14.44	0.690	0.567	21.69
1.000	∞	1.000	1.000	0.00	1.000	1.000	0.00
	25	0.979	0.975	0.41	0.973	0.960	1.35
	10	0.950	0.941	0.96	0.939	0.910	3.19
	5	0.909	0.894	1.68	0.891	0.846	5.32
	2	0.822	0.801	2.62	0.795	0.733	8.46
	1	0.738	0.721	2.36	0.710	0.646	9.91
0.577	∞	1.000	1.000	0.00	1.000	1.000	0.00
	25	0.967	0.864	11.92	0.962	0.956	0.63
	10	0.926	0.839	10.37	0.916	0.907	0.99
	5	0.873	0.809	7.91	0.859	0.850	1.06
	2	0.776	0.755	2.78	0.759	0.766	-0.91
	1	0.699	0.716	-2.37	0.683	0.711	-3.94

Nondimensional Plate Heat Flux: Distributions of $q_p/\bar{q}_p$ are given in Figs. 8(a-e), for the (T) (dashed lines) and (H1) (solid lines) boundary conditions. In all plots, $q_p/\bar{q}_p$ achieves its maximum value at $Y=0$, and decreases monotonically along the plate toward the corner of the duct. In the vicinity of the duct corners, the fluid velocity is lower than that in the region adjacent to the center of the plate ($Y=0$); on the other hand, the fluid temperature in the corners is higher than that in the region adjacent to the center of the plate. Both these phenomena adversely influence the convective heat transfer in the corners, in relation to that at the center of the plate; the plots in Fig. 8 reflect this reasoning.

From Figs. 8(a-e), it is evident that for a fixed aspect ratio, the variation in $q_p/\bar{q}_p$ along the plate for high values of Ω is larger than for low values of Ω. This is because plate-fin ducts with high Ω values, or high fin conductivity, have higher fin temperatures, and hence higher corner fluid temperatures, than those with low Ω values; the closer the fluid temperature is to T_w, the less receptive it is to heat transfer from the plate. Furthermore, the fluid velocity distribution in the region adjacent to the plate is less nonuniform along the plate for high aspect ratio ducts ($\zeta=11.43$ and 3.732) than that for low aspect ratio ducts ($\zeta=0.577$ and 1). Thus, for a fixed value of

Ω, the variation in $q_p/\bar{q}_p$ along the plate for high aspect ratio ducts is somewhat lower than that for low aspect ratio ducts.

Evaluation of the Conventional Approach to the Design of Plate-Fin Ducts. In the conventional approach to the design of plate-fin ducts [1], the less than 100 percent effectiveness of the fin surface is accounted for by using a fin efficiency η_f, and a total surface (plate + fin) efficiency η_0

$$\eta_f = \frac{\text{Actual rate of heat transfer from the fin}}{\text{Rate of heat transfer from the fin when } \Omega = \infty} \tag{29}$$

$$\eta_0 = \frac{\text{Actual rate of heat transfer from the (plate + fin)}}{\text{Rate of heat transfer from the (plate + fin) when } \Omega = \infty} \tag{30}$$

In the conventional approach, these efficiencies are obtained using standard fin theory, in which the surface heat transfer coefficient is assumed to be a constant. For the plate-fin ducts analyzed in this paper, the conventional approach yields

$$\eta_{f,\text{conv}} = \frac{\tanh\,(mL/2)}{(mL/2)}; \quad m = \left(\frac{2h_{\Omega=\infty}}{k_f t}\right)^{1/2}$$
$$\eta_{0,\text{conv}} = 1 - \{L/(L+s)\}(1-\eta_{f,\text{conv}}) \tag{31}$$

In terms of the dimensionless parameters used in this analysis, it can be shown that:

$$\frac{mL}{2} = \left[\frac{\{(\zeta^2+1)^{1/2}+1\}(\zeta^2+1)\text{Nu}_{\Omega=\infty}}{4\zeta^2\Omega}\right]^{1/2}$$
$$\{L/(L+s)\} = (\zeta^2+1)^{1/2}/\{(\zeta^2+1)^{1/2}+1\} \tag{32}$$

The results of the proposed conjugate analysis of plate-fin ducts can be used to calculate the total surface efficiency η_0 as follows

$$\eta_{0,\text{prop}} = \text{Nu}/\text{Nu}_{\Omega=\infty} \tag{33}$$

For laminar fully developed flow and heat transfer, with a given thermal boundary condition and fixed values of ζ and Ω, the average heat transfer coefficient and the corresponding value of η_0 are constant, independent of the Reynolds and Prandtl numbers. Values of $\eta_{0,\text{conv}}$ and $\eta_{0,\text{prop}}$ for all the plate-fin ducts considered in this study, for both the (T) and (HI) boundary conditions, are presented in Table 4. These results show that the conventional approach, for the parameters investigated, can lead to errors in the values of η_0 that range from -8.57 to 29.94 percent.

Concluding Remarks

In this investigation, the heat transfer characteristics of triangular cross section plate-fin ducts have been determined by analyzing conduction in the fin and convection in the fluid, simultaneously, as a conjugate problem. This approach obviates the need for arbitrary assumptions about the heat transfer from the fin surface. The overall and local results presented in this paper highlight the importance of including the fin conductance parameter Ω in the thermal analysis of triangular plate-fin ducts. In addition, they illustrate that the conventional approach to the design of plate-fin ducts, based on the standard fin theory, can lead to significant errors.

Using the data in [1, 2], it may be established that the values of H and t characteristic of plate-fin ducts encountered in compact heat exchangers lie in the following ranges: 2.54 mm $\leq H \leq$ 20.9 mm, and 0.025 mm $\leq t \leq$ 0.254 mm. These values of H and t yield the following ranges of Ω ($=k_f t/kH$): with copper fins ($k_f \simeq 400$ W/m $-$ °C) and air ($k \simeq 0.0263$ W/m $-$ °C), $18.2 \leq \Omega \leq 1521$; with aluminum fins ($k_f \simeq 237$ W/m $-$ °C) and air, $10.8 \leq \Omega \leq 901$; with carbon steel fins ($k_f \simeq 60.5$ W/m $-$ °C) and air, $2.75 \leq \Omega \leq 230$; and with 304 stainless steel ($k_f \simeq 14.9$ W/m $-$ °C) and air, $0.68 \leq \Omega \leq 56.7$. For air-to-air compact heat exchangers, therefore, the results presented in this paper may be used to draw the following conclusions: With copper fins, $T_f \simeq T_w$ throughout the fin, and the results for $\Omega = \infty$ apply; with aluminum, carbon steel, and stainless steel fins, and for fins with $k_f < 200$ W/m $-$ °C, however, it could be erroneous to assume that $T_f \simeq T_w$ throughout the fin, and the results of the conjugate problem analyzed in this paper should be used.

Only triangular plate-fin ducts were investigated in this study. It should be noted, however, that the control-volume numerical method presented in this paper can be easily adapted for the analysis of other plate-fin ducts, such as trapezoidal plate-fin ducts, encountered in compact heat exchangers.

It has been assumed in this work that the triangular plate-fin ducts have sharp corners. In practice, however, soldering, brazing, or welding processes are used to attach the fins to the plates, and the fins may be formed by rolling or cold forging a continuous metal sheet. Thus rounded corners, and imperfect thermal contact between the fins and the plates, could result [1, 2]. An investigation of these effects would be a useful extension of this work. Another interesting and worthwhile extension of this study would be an analysis of developing flow and heat transfer in plate-fin ducts, accounting for axial heat conduction in the fins and the plates. An investigation of turbulent flows and complementary experiments to verify the numerical predictions are also desirable.

Acknowledgments

Financial support from the Natural Sciences and Engineering Research Council of Canada is gratefully acknowledged. Constructive criticism of this work by Dr. R. K. Shah is appreciated.

References

1 Kays, W. M., and London, A. L., *Compact Heat Exchangers*, 3rd ed., McGraw-Hill, New York, 1984.

2 Shah, R. K., and London, A. L., *Laminar Flow Forced Convection in Ducts*, Supplement 1, *Advances in Heat Transfer*, Academic Press, 1978.

3 Kays, W. M., and Crawford, M. E., *Convective Heat and Mass Transfer*, 2nd ed., McGraw-Hill, New York, 1980.

4 Schmidt, F. W., and Newell, M. E., "Heat Transfer in Fully Developed Laminar Flow Through Rectangular and Isosceles Triangular Ducts," *Int. J. Heat Mass Transfer*, Vol. 10, 1967, pp. 1121–1123.

5 Nakamura, H., Hiraoka, S., and Yamada, I., "Laminar Forced Convection Flow and Heat Transfer in Arbitrary Triangular Ducts," *Heat Transfer—Japanese Research*, Vol. 1, 1972, pp. 120–122.

6 Sparrow, E., and Haji-Sheikh, A., "Laminar Heat Transfer and Pressure Drop in Isosceles Triangular, Right Triangular, and Circular Sector Ducts," ASME JOURNAL OF HEAT TRANSFER, Vol. 87, 1965, pp. 426–427.

7 Shah, R. K., "Laminar Flow Friction and Forced Convection Heat Transfer in Ducts of Arbitrary Geometry," *Int. J. Heat Mass Transfer*, Vol. 18, 1975, pp. 849–862.

8 Schneider, G. E., and LeDain, B. L., "Fully Developed Laminar Heat Transfer in Triangular Passages," *J. Energy*, Vol. 5, 1981, pp. 15–21.

9 Sparrow, E. M., Baliga, B. R., and Patankar, S. V., "Forced Convection Heat Transfer From a Shrouded Fin Array With and Without Tip Clearance," ASME JOURNAL OF HEAT TRANSFER, Vol. 100, 1978, pp. 572–579.

10 Soliman, H. M., Chau, T. S., and Trupp, A. C., "Analysis of Laminar Heat Transfer in Internally Finned Tubes With Uniform Outside Wall Temperature," ASME JOURNAL OF HEAT TRANSFER, Vol. 102, 1980, pp. 598–604.

11 Sparrow, E. M., and Lee, L., "Effects of Fin Base-Temperature Depression in a Multifin Array," ASME JOURNAL OF HEAT TRANSFER, Vol. 97, 1975, pp. 463–465.

12 Heggs, P. J., and Stones, P. R., "The Effects of Dimensions on the Heat Flowrate Through Extended Surfaces," ASME JOURNAL OF HEAT TRANSFER, Vol. 102, 1980, pp. 180–182.

13 Sparrow, E. M., and Patankar, S. V., "Relationships Among Boundary Conditions and Nusselt Numbers for Thermally Developed Duct Flows," ASME JOURNAL OF HEAT TRANSFER, Vol. 99, 1977, pp. 483–485.

14 Baliga, B. R., and Patankar, S. V., "A New Finite-Element Formulation for Convection-Diffusion Problems," *Numerical Heat Transfer*, Vol. 3, 1980, pp. 393–409.

15 Segerlind, L. J., *Applied Finite Element Analysis*, Wiley, New York, 1976.

16 Patankar, S. V., *Numerical Heat Transfer and Fluid Flow*, Hemisphere, Washington, D.C., 1980.